Thermal conductivity tensors of the cladding and active layers of antimonide infrared lasers and detectors

Chuanle Zhou,[1] I. Vurgaftman,[2] C. L. Canedy,[2] C. S. Kim,[2] M. Kim,[4] W. W. Bewley,[2] C. D. Merritt,[2] J. Abell,[2] J. R. Meyer,[2] A. Hoang,[3] A. Haddadi,[3] M. Razeghi,[3] and M. Grayson[1,*]

[1]*Electrical Engineering and Computer Science, Northwestern University, Evanston, IL 60208*
[2]*Code 5613, Naval Research Laboratory, Washington DC 20375*
[3]*Center for Quantum Devices, Electrical Engineering and Computer Science, Northwestern University, Evanston, IL 60208*
[4]*Sotera Defense Solutions, Inc., Crofton MD 21114*
[*]*m-grayson@northwestern.edu*

Abstract: The in-plane and cross-plane thermal conductivities of the cladding layers and active quantum wells of interband cascade lasers and type-II superlattice infrared detector are measured by the 2-wire 3ω method. The layers investigated include InAs/AlSb superlattice cladding layers, InAs/GaInSb/InAs/AlSb W-active quantum wells, an InAs/GaSb superlattice absorber, an InAs/GaSb/AlSb M-structure, and an AlAsSb digital alloy. The in-plane thermal conductivity of the InAs/AlSb superlattice is 4-5 times higher than the cross-plane value. The isotropic thermal conductivity of the AlAsSb digital alloy matches a theoretical expectation, but it is one order of magnitude lower than the only previously-reported experimental value.

OCIS codes: (140.6810) Thermal effects, (140.5960) Semiconductor lasers, (260.3060) Infrared,(310.6870) Thin films, other properties.

References and links

1. S. Abdollahi Pour, E.K. Huang, G. Chen, A. Haddadi, B.M. Nguyen and M. Razeghi, "High operating temperature midwave infrared photodiodes and focal plane arrays based on Type-II InAs/GaSb superlattices," Appl. Phys. Lett., **98**, 143501 (2011).
2. E.K. Huang, M.A. Hoang, G. Chen, S.R. Darvish, A. Haddadi, and M. Razeghi, "Highly selective two-color midwave and long-wave infrared detector hybrid based on Type-II superlattices," Optics Letters, **37**, 4744 (2012).
3. D. Caffey, T. Day, C. S. Kim, M. Kim, I. Vurgaftman, W. W. Bewley, J. R. Lindle, C. L. Canedy, J. Abell, and J. R. Meyer, "Performance characteristics of a continuous-wave compact widely tunable external cavity interband cascade lasers," Optics Letters, **18**, 15691 (2010).
4. I. Vurgaftman, W. W. Bewley, C. L. Canedy, C. S. Kim, M. Kim, J. R. Lindle, C. D. Merritt, J. Abell, and J. R. Meyer, "Mid-IR Type-II interband cascade lasers," IEEE J. Sel. Topics Quantum Electron., **17**, 1435 (2011).
5. C. Zhou, S. Birner, Yang Tang, K. Heinselman, and M. Grayson, "Driving perpendicular heat flow: $p \times n$ type transverse thermoelectrics for microscale and cryogenic peltier cooling," Phys. Rev. Lett. **110**, 227701 (2013).
6. T. Borca-Tasciuc, D. Achimov, W. L. Liu, G. Chen, H.-W. Ren, C.-H. Lin, and S. S. Pei, "Thermal conductivity of InAs/AlSb superlattices," Microscale Thermophysical Engineering **5** 225 (2001).
7. Borca-Tasciuc, T., Kumar, A. R., and Chen, G., "Data reduction in 3ω method for thin-film thermal conductivity determination," Rev. Sci. Instrum., **72**, 2139 (2001).
8. T. Borca-Tasciuc, D. W. Song, J. R. Meyer, I. Vurgaftman, M.-J. Yang, B. Z. Nosho, and L. J. Whitman, H. Lee and R. U. Martinelli, G. W. Turner and M. J. Manfra and G. Chen, "Thermal conductivity of $AlAs_{0.07}Sb_{0.93}$ and $Al_{0.9}Ga_{0.1}As_{0.07}Sb_{0.93}$ alloys and $(AlAs)_1/(AlSb)_1$1 digital-alloy superlattices," J. Appl. Phys., **92**, 4994 (2002).

#193146 - $15.00 USD Received 1 Jul 2013; revised 5 Aug 2013; accepted 5 Aug 2013; published 6 Sep 2013

9. C. Zhou, B.-M. Nguyen, M. Razeghi, M. Grayson, "Thermal conductivity of InAs/GaSb Superlattice," J. Elect. Mat., **41**, 2322 (2012).
10. C. Zhou, G. Koblmuller, M. Bichler, G. Abstreiter, M. Grayson, "Thermal conductivity tensor of semiconductor layers using two-wire 3ω method," Proc. of SPIE, **8631**, 863129 (2013).
11. J. Garg, N. Bonini and N. Marzari, "High thermal conductivity in short-period superlattices," Nano Lett., **11**, 5135 (2011).

1. Introduction

III-V antimonide infrared (IR) detectors typically operate cryogenically [1, 2], whereas the latest generation of midwave IR (mid-IR) lasers operates at room temperature [3, 4]. However, both performances degrade rapidly with increasing temperature. So to enable optimization, it is important to identify the most critical thermal bottlenecks in the device structures so that the net thermal resistance can be minimized and the heat dissipation can be maximized. T2SLs have also been reported recently as a possible new class of transverse thermoelectric material, in which low thermal conductivity would actually be advantageous [5].

In particular, the maximum continuous-wave (cw) output power and operating temperature [3] of a mid-IR interband cascade laser (ICL) [4] is limited by the thermal impedance. The ICL consists of a thin active core (200-300 nm) sandwiched between somewhat thicker GaSb separate-confinement layers, which are in turn enclosed by top (1-1.5 μm thick) and bottom (3-4 μm thick) InAs/AlSb superlattice (SL) cladding layers. The processed ICL ridge is then coated with a thick layer of electroplated Au and mounted epitaxial-side-down on a heat sink [3]. Thermal simulations indicate that in this scenario, the most significant thermal bottleneck is the cross-plane thermal conductivity of the InAs/AlSb SL comprising the top cladding. This physical quantity has been investigated in one previous publication [6], although not for the SL layer thicknesses employed in current state-of-the-art ICL designs. The thermal impedance of the narrowest ICL ridges (width less than 10-15 μm) is also quite sensitive to the thermal conductivity of the insulator deposited on the ridge sidewalls. The thermal impedance is less sensitive to the in-plane thermal conductivity of the InAs/AlSb SL, although in cases where the insulator does not present a significant thermal barrier the in-plane heat flow assumes greater importance. It seems reasonable to assume that the active core of the ICL (InAs/GaInSb/InAs/AlSb repeated layers), the bulk of of which consists of an InAs/AlSb electron injector, is thermally similar to the cladding SL. The accuracy of this assumption will require verification in the future, however, and its effect on the ICL thermal impedance may become greater for ICLs with more stages for higher cw output power.

A closely-related antimonide heterostructure is the InAs/GaSb type-II superlattice (T2SL) that has been used successfully to suppress dark currents and improve the detectivities of mid-IR and long-wavelength (LWIR) photodiodes (PDs) [1]. However, because the dark currents of mid-IR and LWIR PDs and detectors can increase by several orders of magnitude with temperature [2], it is important to calibrate the thermal conductivities of the active and barrier layers. For example, an InAs/GaSb T2SL with 39.6/21.3 Å is used for the active region of an LWIR PD with 50% cut-off around 11 μm. An InAs/GaSb/AlSb/GaSb M-structure is then used for the barriers in LWIR p-pi-M-N heterostructure as well as mid-IR T2SL detectors. In addition, InAsSb with composition lattice-matched to GaSb serves as a chemically-selective etch-stop layer in IR PDs.

In this work, we have measured the in-plane and cross-plane thermal conductivities of a variety of short-period antimonide heterostructure device components using the 2-wire 3ω method [7]. The investigated structures include InAs/AlSb cladding layers and InAs/GaInSb/InAs/AlSb W quantum wells (QWs) of ICLs, the InAs/GaSb LWIR active absorber region and InAs/GaSb/AlSb M-structure of T2SL PDs, InAsSb and an AlAsSb digital alloy insulating layer. While the cross-plane thermal conductivities of InAs/AlSb SLs [6],

#193146 - $15.00 USD Received 1 Jul 2013; revised 5 Aug 2013; accepted 5 Aug 2013; published 6 Sep 2013

AlAsSb digital alloys [8], and T2SLs [9] have been measured previously, to the best of our knowledge the in-plane thermal conductivities have never been reported.

2. Experiment

The four samples studied in this work, which were grown at NRL and Northwestern by molecular beam epitaxy on GaSb substrates, are specified in Table 1. Sample A is a thin ICL cladding structure, consisting of a 0.5-μm $(AlAs)_1/(AlSb)_{12.5}$ digital alloy buffer layer, followed by a 1-μm InAs/AlSb (24.3/23 Å) SL, and an n-doped 10-nm InAs capping layer. Sample B is a thick ICL cladding structure, consisting of a 7-μm-thick InAs/AlSb SL (24.3/23 Å) on a GaSb substrate. Sample C consists of InAs/GaInSb/InAs/AlSb repeated W-active QWs with total thickness 0.485 μm. Sample D is an InAs/GaSb T2SL structure, comprising a 0.5-μm InAsSb alloy buffer layer followed by a 0.67-μm-thick InAs/GaSb (39.6/21.3 Å) T2SL and 0.2-μm-thick InAs/GaSb/AlSb/GaSb (54.9/9.1/15.2/9.1 Å) M-structure.

The 3ω method uses metal filaments deposited on the sample as both heaters and thermometers. An AC current $I(\omega)$ can heat up the filament by $\Delta T(2\omega)$, which is proportional to the measured third harmonic voltage $V_{3\omega}$. The sample thermal conductivity can be deduced from the frequency dependent $\Delta T(2\omega)$. To prepare for the 3ω method measurement, we first etched the layer of interest from half of the sample area. For Samples A (thin ICL cladding) and D (T2SL), both of which contained multiple layers of interest, we etched the samples into several steps, as shown in the inset of Fig. 1(a). Then we used PECVD to deposit $d^{\mathrm{SiN_x,f}}$ = 60 nm of SiN_x as an insulating layer, followed by the deposition of 200-nm-thick Au filaments to serve as both heaters and thermometers. One wide filament of $2b$ = 30 μm and one narrow filament of $2b$ = 2 μm were deposited on the film, the buffer layer and the substrate. For the thick cladding sample, one narrow Ni filament of $2b$ = 4 μm was deposited on both the film and the substrate, as shown in the inset of Fig. 1(b). Calibrated with the same 3ω method, the PECVD-deposited SiN_x has a higher thermal conductivity (1.5-1.9 W/m·K) than a sputtered dielectric layer (<1 W/m·K), and 60 nm of SiN_x is thick enough to insulate as well as a much thicker SiO_2 layer. Therefore, the SiN_x layer induces minimal temperature rise in the 3ω measurement for improved accuracy. The filament widths were chosen such that the wide filaments were much wider than film thickness to ensure 1D heat transport, while the widths of the narrow filaments were about the same as the film thickness to increase the accuracy of the in-plane thermal conductivity measurement.

We first measured the 30-μm-wide filament to determine the substrate thermal conductivity $\kappa^{\mathrm{GaSb,sub}}$ and the cross-plane thermal conductivity of the films κ^{f}_{yy}:

$$\kappa^{\mathrm{GaSb,sub}} = -\frac{P}{2\pi l}\frac{d(\ln\omega)}{d(\Delta T)}, \tag{1}$$

$$\kappa^{\mathrm{f}}_{yy} = \frac{P d^{\mathrm{f}}}{2b\,l\,\Delta T^{\mathrm{f}}} \tag{2}$$

where P is the power applied to the heater, and l is the length of the Au filament. $\Delta T^{\mathrm{f}} = \Delta T^{\mathrm{f+s}} - \Delta T^{\mathrm{s}}$, where $\Delta T^{\mathrm{f+s}}$ and ΔT^{s} are the temperature oscillation amplitude of the Au filament on the film-plus-substrate and on the substrate alone, respectively.

We then used the two narrow filaments to determine the cross-plane and in-plane thermal conductivities of the thin films. The heater temperature oscillation amplitude can be calculated with the iterative equation

$$\Delta T = \frac{-P}{\pi l \kappa_{yy1}}\int_0^\infty \frac{1}{A_1 B_1}\frac{\sin^2(b\lambda)}{(b^2\lambda^2)}d\lambda, \tag{3}$$

#193146 - $15.00 USD Received 1 Jul 2013; revised 5 Aug 2013; accepted 5 Aug 2013; published 6 Sep 2013

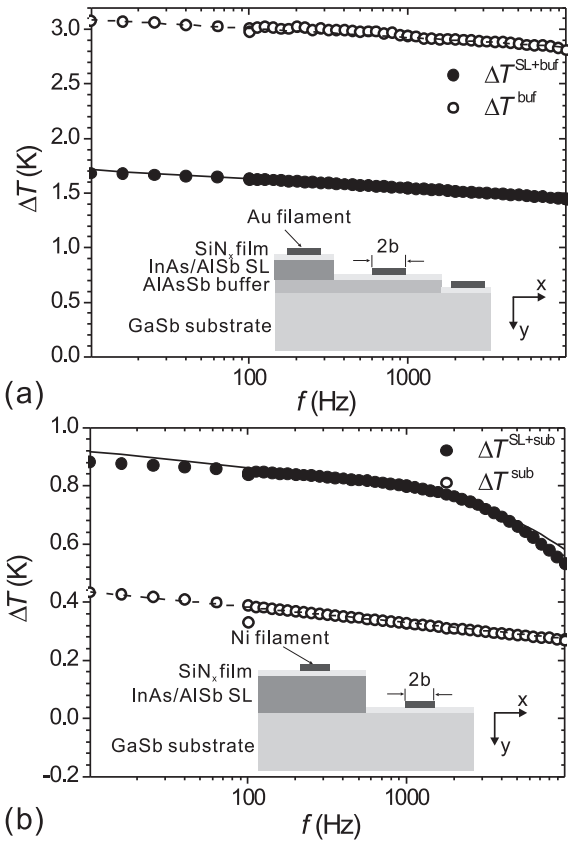

Fig. 1. Measured frequency-dependent temperature rise ΔT of the narrow filaments on the thin film (solid circles) and on the substrate (open circles) of Samples A (thin cladding) and B (thick cladding). The fitted ΔT of the filaments on the thin film and substrate are shown in solid lines and dashed lines, respectively. The insets show the cross-sectional layer structures of the samples. (a) For Sample A, the wide filaments on the buffer layer and the substrate were used to measure the cross-plane thermal conductivity of the buffer layer, while the narrow filaments on the buffer layer and the SL were used to measure the in-plane and cross-plane thermal conductivity of the InAs/AlSb superlattice. (b) For Sample B, the narrow filaments on the substrate and the SL were used to measure the in-plane and cross-plane thermal conductivities of the InAs/AlSb superlattice. Samples C and D were measured in a similar manner, using multiple etch steps with Au filaments at each step for each individual layer.

#193146 - $15.00 USD Received 1 Jul 2013; revised 5 Aug 2013; accepted 5 Aug 2013; published 6 Sep 2013

where n is the total number of layers, the index i layer starting from the top, and

$$A_{i-1} = \frac{A_i \frac{\kappa_{yyi} B_i}{\kappa_{yyi-1} B_{i-1}} - \tanh(\phi_{i-1})}{1 - A_i \frac{\kappa_{yyi} B_i}{\kappa_{yyi-1} B_{i-1}} \tanh(\phi_{i-1})}, i = 2...n \tag{4}$$

is an iterative parameter, the value of which for the upper layer is calculated from that of the lower layers, and A_n=-1 for the semi-infinite substrate.

$$B_i = \left(\frac{\kappa_{xx}}{\kappa_{yy}} \lambda^2 + \frac{\mathrm{i}2\omega}{\alpha_{yyi}} \right)^{1/2} \tag{5}$$

with the unit of wave number is related to the anisotropic thermal diffusivity of the ith layer, λ is an integration variable with the unit of wave number, the dimensionless variable $\phi_i = B_i d_i$ is related to the anisotropic heat flow within a finite layer thickness, and $\alpha = \kappa/\rho C_\mathrm{p}$ is the thermal diffusivity. We estimated all the fit parameters in Eq. (3) based on literature values (κ, ρ and C_p) or measured values (b, $d^{\mathrm{SiN_x}}$, $\kappa_{yy}^{\mathrm{SiN_x}}$, $\kappa^{\mathrm{GaSb,sub}}$ and κ_{yy}^{f}) and use the iterative equation to calculate the heater temperature oscillation amplitude ΔT. Fig. 1 shows the fitted curves (lines) and measured data (circles) of Samples A (thin cladding) and B (thick cladding).

To quantify the measurement error, we calculated the error for various fit parameters by varying the parameter values by 20% from their best fit and summing the squared error: [10]

$$\varepsilon = \sum_j \Delta(\ln \omega_j)[\Delta T^{\mathrm{fit}}(\omega_j) - \Delta T(\omega_j)]^2, \Delta(\ln \omega_j) = \ln(\omega_j/\omega_{j-1}) \tag{6}$$

where $\Delta T^{\mathrm{fit}}(\omega_j)$ and $\Delta T(\omega_j)$ are the fitted and measured ΔT at the angular frequency ω_j, respectively. The best fit value for each parameter gives the smallest total error ε in units of K^2.

3. Results and Discussion

Table 1. Thermal conductivity tensor components at 300 K. The data from the present study are listed (black). Literature values are cited with references numbers in brackets (grey).

Layers	d^{f} (μm)	SL Period (Å)	(ML)	κ_{yy} (W/m·K)	κ_{xx} (W/m·K)
InAs/GaSb T2SL	0.67	39.6/21.3	13/7	4.9 ± 1	10 ± 2
[9]	3.0	36.6/24.4	12/8	3.1± 0.8	–
	3.0	57.9/54.9	19/18	4.8 ± 1	–
M-structure	0.2	54.9/9.1/15.2/9.1	18/3/5/3	5.8 ± 0.5	–
InAsSb alloy	0.5	–	–	15 ± 4	15 ± 4
W-QWs	0.485	17/30/15/14	6/10/5/5	1.3 ± 0.2	4.5 ± 0.9
InAs/AlSb SL	1.0	24.3/23	8/8	2.7 ± 0.3	13 ± 2.5
	7.0	24.3/23	8/8	2.7 ± 0.14	10.9 ± 1.1
[6]	1.0	33.4/31.8	11/10	3 ± 0.3	–
$(AlAs)_1/(AlSb)_{12.5}$	0.5	2.8/38.3	1/12.5	0.49 ± 0.02	0.49 ± 0.1
$(AlAs)_1/(AlSb)_{11}$ [8]	1.0	2.8/33.7	1/11	7.3 ± 0.7	–
(Theory)[8]	1.0	2.8/33.7	1/11	0.35-2.0	–

The error analyses are shown in Fig. 2, in which the errors for the in-plane and cross-plane thermal conductivities of the layer of interest are plotted as solid curves and for other fit parameters are plotted as dashed curves. The widths of the narrow filaments are the most important fit

#193146 - $15.00 USD Received 1 Jul 2013; revised 5 Aug 2013; accepted 5 Aug 2013; published 6 Sep 2013

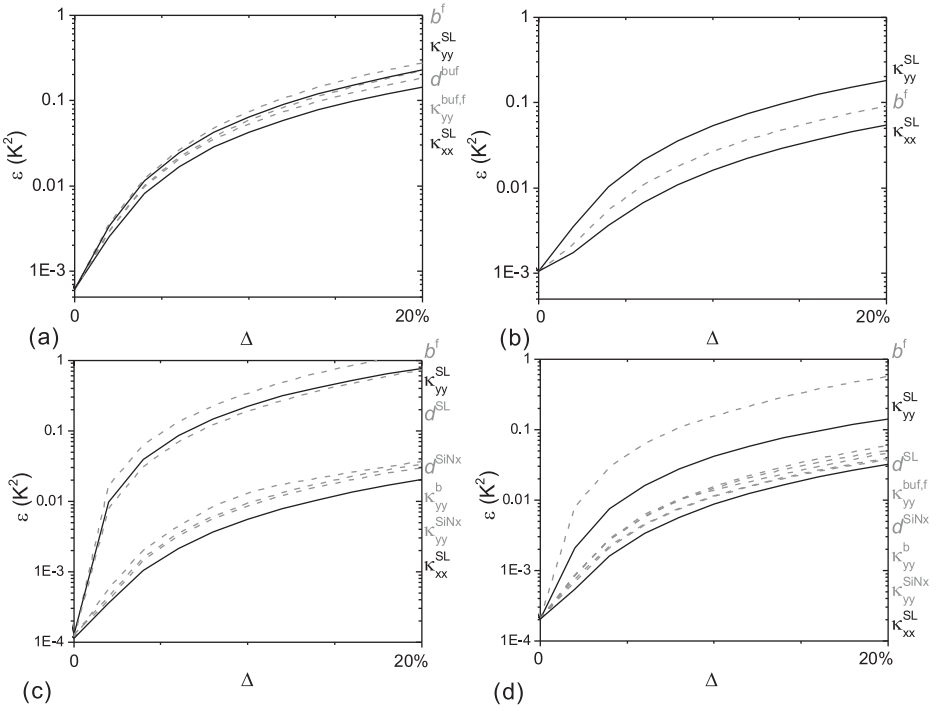

Fig. 2. Following the error analysis method of Ref. [10], plot of the mean-squared fitting error ε for the narrow filament data calculated from Eq. (6) when the value of each fit parameter is varied by 20% around the global minimum error. Only the parameters with errors greater than 0.01 K^2 mean-squared error are plotted for the error analysis. Thermal conductivities for the layers of interest are plotted in solid lines and other fit parameters are plotted in dashed lines. The parameters' names are listed on the right of each plot in the same sequence as the curves. (a) 2 μm Au filament on Sample A (thin cladding). (b) 4 μm Ni filament on the superlattice of Sample B (thick cladding). (c) 2 μm Au filament on the superlattice of Sample C (W-active). (d) 2 μm Au filament on the superlattice of Sample D (T2SL).

#193146 - $15.00 USD Received 1 Jul 2013; revised 5 Aug 2013; accepted 5 Aug 2013; published 6 Sep 2013

parameters for all the samples, the uncertainty of which depends on the lithography and lift-off quality. For each multilayer sample, the fitted thermal conductivity also depends on the actual thicknesses of the thin film of interest and the buffer layer underneath it.

For the ICL samples, the uncertainties of the in-plane thermal conductivity determined for the InAs/AlSb SL in Sample A (thin cladding) and the InAs/GaInSb/InAs/AlSb W-active QWs for Sample C are about 20%, while it is about 10% for the InAs/AlSb SL in Sample D (thick cladding). The uncertainties for the in-plane thermal conductivities are larger for the former two samples because their narrow filament widths are larger than the superlattice thickness, whereas the narrow filament width is smaller than the SL thickness for the thick cladding sample. The uncertainty of about 20% for the AlAsSb digital alloy depends on the uncertainties of the width of the narrow filament $2b$, the thickness of the alloy buffer layer d^{buf}, and the cross-plane thermal conductivity of the superlattice layer $\kappa_{yy}^{\mathrm{InAs/AlSbSL,f}}$. For Sample D, the uncertainty for the InAs/GaSb T2SL in-plane thermal conductivity is about 20%, depending on the accuracies of the thickness and cross-plane thermal conductivity of the InAsSb buffer layer.

The measurement results are shown in Fig. 3 and Table. 1. The cross-plane thermal conductivity of the InAs/GaSb T2SL and the M-structure are 4.9 W/m·K and 5.77 W/m·K, respectively. These values are of the same order as our previous measurements of T2SLs with larger superlattice periods [9]. The cross-plane thermal conductivity of the InAs/AlSb superlattice $\kappa_{yy}^{\mathrm{InAs/AlSbSL,f}}$ is 2.7 W/m·K from measurements on both the thin and thick cladding samples. This $\kappa_{yy}^{\mathrm{InAs/AlSbSL,f}}$ also matches a previous measurement for an InAs/AlSb SL grown at 460°C [6]. The in-plane thermal conductivities determined for the InAs/AlSb SL from the two samples are 13.1 W/m·K and 10.9 W/m·K, respectively. The smaller in-plane thermal conductivity of sample B could result from the accumulated interface roughness in the thick cladding sample. The measured anisotropies are greater for the InAs/AlSb SLs than for the InAs/GaSb T2SL.

The measured thermal conductivity of the $(\mathrm{AlAs})_1/(\mathrm{AlSb})_{12.5}$ digital alloy $\kappa^{\mathrm{AlAsSb,f}}$ is 0.49 W/m·K and isotropic. The same value is measured both with the wide filament and the narrow filament of the two-wire 3ω method, and this very low thermal conductivity matches the totally-diffuse prediction of the thermal boundary resistance (TBR) calculation of Ref. [8]. However, Ref. [8] also provides the only previous measurement of thermal conductivity on a similar $(\mathrm{AlAs})_1/(\mathrm{AlSb})_{11}$ digital alloy and reports an order of magnitude higher value than ours, which is also an order of magnitude higher than their TBR calculation [8]. The authors in Ref. [8] explain the discrepancy between their experimental value and the TBR calculation as possibly due to phonon tunneling through the thin AlAs layer, and recent studies showed that short-period superlattices may have high thermal conductivities [11]. Yet our sample has the same thickness of AlAs layer as this previous work, so this cannot explain the discrepancy with our result. Given the consistency of our wide and narrow filament measurements and the careful error analysis which we explain in this work, we believe that we have ample evidence to justify reporting this result.

4. Conclusion

We measured and analyzed thermal conductivity tensors and their uncertainties for the cladding layer and active quantum wells of mid-IR interband cascade lasers, the active absorber and "M" barrier layers of mid-IR and LWIR photodiodes, and an AlAsSb insulating buffer layer. The cross-plane thermal conductivities determined for the various SLs agree well with previous measurements. The low thermal conductivity of the AlAsSb digital alloy matches a TBR calculation, although it is more than an order of magnitude lower than a previous experimental finding.

While a full comparison of the experimental thermal-impedance values for interband cascade laser structures with finite-element simulations of the heat conduction will be reported

#193146 - $15.00 USD Received 1 Jul 2013; revised 5 Aug 2013; accepted 5 Aug 2013; published 6 Sep 2013

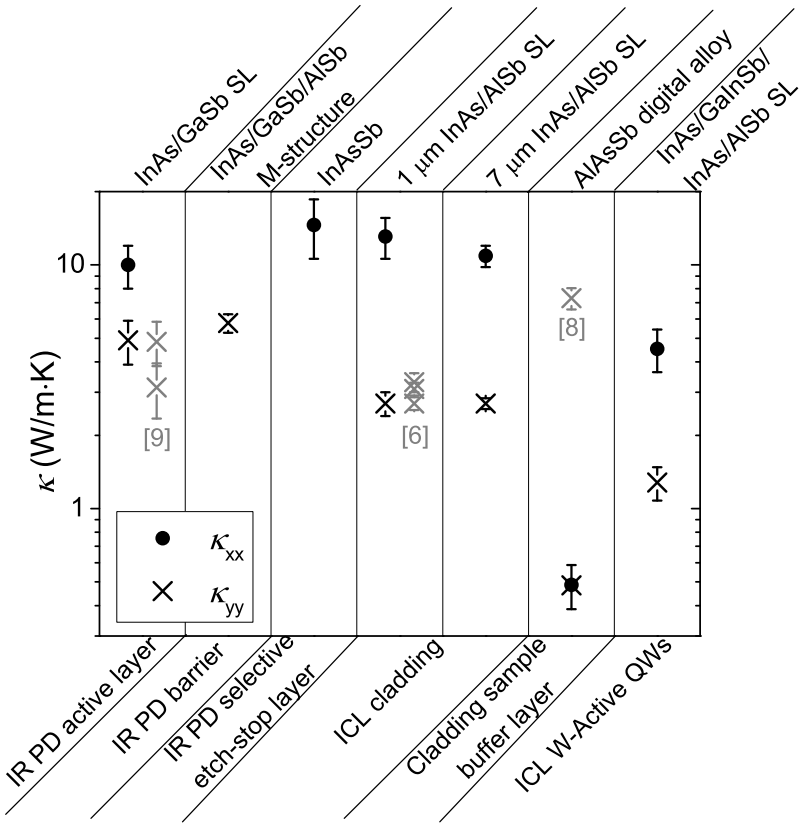

Fig. 3. In-plane (solid circles) and cross-plane (crosses X) thermal conductivities for the T2SL, M-structure, 1-μm InAs/AlSb SL, 7-μm InAs/AlSb SL, AlAsSb digital alloy, and InAs/GaInSb/InAs/AlSb W QWs, compared to previously published values in grey (reference numbers indicated next to the data points).

elsewhere, that modeling is broadly consistent with InAs/AlSb SL cross-plane thermal conductivities in the 2-3 W/m·K range when the insulator thermal conductivity of 1.7 W/m·K derived in the present work is employed. The thermal conductivity tensors obtained from the present study imply a net thermal impedance only $<10\%$ lower than the experimental value derived from characterization of an 8-μm-wide epi-down-mounted ICL ridge. It should be emphasized that a precise fit would require full incorporation of all the minor structural details of the processed ICL structure, and assuming the absence of any thermal bottleneck at the bonded device/heat-sink interface. In view of these uncertainties, the agreement with the results of the present work is quite good. The fits are much less sensitive to the SL in-plane thermal conductivity than the cross-plane value, owing to the poor conductance of the insulator layer and the presence of highly-conductive GaSb layers in the structure.

Acknowledgments

The work at Northwestern was supported by AFOSR grants FA-9550-09-1-0237 and FA-9550-12-1-0169, Initiative for Sustainability and Energy at Northwestern (ISEN) and NSF MRSEC

#193146 - $15.00 USD Received 1 Jul 2013; revised 5 Aug 2013; accepted 5 Aug 2013; published 6 Sep 2013

grants No. DMR-0520513 and No. DMR-0748856 through both instrumentation grants and an NSF MRSEC Fellowship. Work at NRL was supported by ONR.

#193146 - $15.00 USD Received 1 Jul 2013; revised 5 Aug 2013; accepted 5 Aug 2013; published 6 Sep 2013